



Article

Optimizing the Properties of $\text{La}_{0.8}\text{Sr}_{0.2}\text{CrO}_3$ Thin Films through Post-Annealing for High-Temperature Sensing

Dan Liu ^{1,2,*} , Peng Shi ^{2,*} , Yantao Liu ³, Yijun Zhang ², Bian Tian ⁴ and Wei Ren ²

¹ Key Laboratory of Instrumentation Science & Dynamic Measurement, Ministry of Education, North University of China, Taiyuan 030051, China

² Electronic Materials Research Laboratory, Key Laboratory of the Ministry of Education & International Center for Dielectric Research, School of Electronic and Information Engineering, Xi'an Jiaotong University, Xi'an 710049, China; zhangyj518@mail.xjtu.edu.cn (Y.Z.); wren@mail.xjtu.edu.cn (W.R.)

³ Department of Electronic Engineering, Xi'an University of Technology, Xi'an 710048, China; liuytxjtu@163.com

⁴ State Key Laboratory for Mechanical Manufacturing Systems Engineering, School of Mechanical Engineering, Xi'an Jiaotong University, Xi'an 710049, China; t.b12@mail.xjtu.edu.cn

* Correspondence: liudan235@nuc.edu.cn (D.L.); spxjy@mail.xjtu.edu.cn (P.S.)

Abstract: $\text{La}_{0.8}\text{Sr}_{0.2}\text{CrO}_3$ (0.2LSCO) thin films were prepared via the RF sputtering method to fabricate thin-film thermocouples (TFTCs), and post-annealing processes were employed to optimize their properties to sense high temperatures. The XRD patterns of the 0.2LSCO thin films showed a pure phase, and their crystallinities increased with the post-annealing temperature from 800 °C to 1000 °C, while some impurity phases of Cr_2O_3 and SrCr_2O_7 were observed above 1000 °C. The surface images indicated that the grain size increased first and then decreased, and the maximum size was 0.71 μm at 1100 °C. The cross-sectional images showed that the thickness of the 0.2LSCO thin films decreased significantly above 1000 °C, which was mainly due to the evaporation of Sr^{2+} and Cr^{3+} . At the same time, the maximum conductivity was achieved for the film annealed at 1000 °C, which was 6.25×10^{-2} S/cm. When the thin films post-annealed at different temperatures were coupled with Pt reference electrodes to form TFTCs, the trend of output voltage to first increase and then decrease was observed, and the maximum average Seebeck coefficient of 167.8 $\mu\text{V}/^\circ\text{C}$ was obtained for the 0.2LSCO thin film post-annealed at 1100 °C. Through post-annealing optimization, the best post-annealing temperature was 1000 °C, which made the 0.2LSCO thin film more stable to monitor the temperatures of turbine engines for a long period of time.

Keywords: post-annealing; $\text{La}_{0.8}\text{Sr}_{0.2}\text{CrO}_3$; thin-film thermocouple; high-temperature sensing



Citation: Liu, D.; Shi, P.; Liu, Y.; Zhang, Y.; Tian, B.; Ren, W. Optimizing the Properties of $\text{La}_{0.8}\text{Sr}_{0.2}\text{CrO}_3$ Thin Films through Post-Annealing for High-Temperature Sensing. *Nanomaterials* **2021**, *11*, 1802. <https://doi.org/10.3390/nano11071802>

Academic Editor:
Christophe Detavernier

Received: 21 June 2021
Accepted: 9 July 2021
Published: 11 July 2021

Publisher's Note: MDPI stays neutral with regard to jurisdictional claims in published maps and institutional affiliations.



Copyright: © 2021 by the authors. Licensee MDPI, Basel, Switzerland. This article is an open access article distributed under the terms and conditions of the Creative Commons Attribution (CC BY) license (<https://creativecommons.org/licenses/by/4.0/>).

1. Introduction

The gas turbine engine at the heart of the airplane is a highly complex and precise thermal machinery, where its working temperature needs to be monitored in real time and in situ to reflect the operational conditions for designing constructions or warning states of modern propulsion systems; however, it is difficult to obtain operating temperatures accurately with available technologies due to the extreme conditions [1]. Various noncontacting sensing technologies have been employed, such as optic pyrometers [2] and acoustic pyrometers [3], but the measuring temperature of turbine engines is not direct and accurate, due to the principles of these technologies, and their complicated structures and sensing modules do not make them easy to integrate with the turbine engine. However, thin-film thermocouples (TFTCs) as a typical kind of immersive sensor can be deposited directly onto the surfaces of turbine engine components with a thickness of a few micro/nanometers using modern deposition technologies; they have been promising as thermal sensors for turbine engines due to the advantages of excellent spatial resolution, cost-effective in large quantities, and rapid response [4–8].

TFTCs consist of two beams that should have excellent oxidation resistance and chemical stability because of the high working temperature in air, and the two beams should have large and stable Seebeck coefficients to form a TFTC with higher sensitivity. It is well-known that a wire-type thermocouple fabricated by conventional noble metals, such as Pt, Rh, or their alloys, can be used to measure high temperatures in air, which can even endure up to about 1820 °C with Al₂O₃ shield protection [9]. Conversely, the maximum measurement temperature is only 1100 °C when it is changed into a thin film, which is mainly ascribed to the coalescence reaction between the TFTC and substrate, and the oxidation of rhodium above 800 °C [10,11]. In addition, its sensitivity is lower due to the small intrinsic Seebeck coefficients of noble metals. Therefore, the development of a new TFTC fabricated by conductive ceramics has been a trend to measure high temperatures in air [12–15]. Especially, conductive oxides with better oxidation resistance and higher Seebeck coefficients have become the most promising candidate materials of electrodes for TFTCs, such as In₂O₃, ITO, ZnO:Al (AZO), and La_{1-x}Sr_xCrO₃ (xLSCO) [14,16–19]. When In₂O₃ and ITO were used to fabricate the electrodes of TFTCs, they had excellent performances with a maximum measurement temperature of 1280 °C, while a serious volatilization problem appeared for them above 1200 °C especially because of the losing of Sn⁴⁺ from ITO, and the indium element is scarce in the earth [20–22]. Meanwhile, for xLSCO, wider applications in the energy and sensor fields of the present materials in the thin films field have also been reported in recent years. They are suitable for interconnect materials in solid oxide fuel cells [23–25], transparent electrolytes and electrodes of batteries and generators [26–30], thin-film fluorescent sensors, and high-temperature sensing [17,18,31,32], with their high melting point of 2490 °C, good conductivity, and high Seebeck coefficient. From our previous work [17], a screen-printed thick-film thermocouple fabricated by LaCrO₃ (LCO) and La_{0.8}Sr_{0.2}CrO₃ can be used to measure a temperature of 1550 °C for 10 h in air, which has inspired the fabrication of TFTCs by using xLSCO electrodes. Since then, some TFTCs fabricated by the 0.2LSCO thin film have been investigated, such as 0.2LSCO-In₂O₃ [19] and 0.2LSCO-Pt [33], with a higher sensitivity and stable output voltage versus the temperature difference. However, the properties of 0.2LSCO thin films can be affected significantly by the post-annealing treatment process, which have not yet been investigated systematically and should be studied to fabricate TFTCs with a stable output voltage curve to use at high temperatures.

In this paper, 0.2LSCO thin films were fabricated successfully via the RF sputtering method. The effects of different post-annealing temperatures on the microstructures, morphologies, and electrical conductivities of 0.2LSCO thin films were investigated systematically. Then, the thermoelectric properties of 0.2LSCO thin films were studied by coupling with platinum (Pt) reference electrodes at a static calibration system. Finally, the optimal post-annealing temperature was obtained by comprehensive analysis.

2. Experimental Sections

A La_{0.8}Sr_{0.2}CrO₃ target was used to deposit the 0.2LSCO thin films onto alumina substrates with sizes of 100 mm × 20 mm × 1 mm via the RF sputtering method. A JDP-560 model sputtering system (Sky Technology Development Co., Ltd., Shen yang, China) was used to deposit the thin films. The detailed deposition processes were the same as our previous work [33]. Before the deposition of the thin films, the alumina substrates were cleaned by ultrasonication with acetone, ethyl alcohol, and deionized water, successively. Then, the 0.2LSCO thin films were deposited on cleaned alumina substrates by the RF sputtering system at 500 °C. Finally, the as-deposited thin films were post-annealed at different temperatures from 800 °C to 1300 °C for 1 h with an interval of 100 °C.

A Dmax/1400 X-ray diffractometer (Rigaku, Tokyo, Japan, Cu K α radiation) was used to characterize the crystal structures of 0.2LSCO thin films with a step of 0.02°. The surface and cross-sectional SEM images were obtained by a FEI Quanta 250 FEG field-emission scanning electron microscope (FEI, Hillsboro, OR, USA), and the composition of elements in the thin films was analyzed by an energy-dispersive spectrometer. The

conductivities of 0.2LSCO thin films were measured by the four-point probe method using the Vanderbilt law.

To characterize the thermoelectric properties of the 0.2LSCO thin films, they were sputtered to form L patterns using the photolithography technique, and then post-annealed at different temperatures for 1 h. Subsequently, another electrode of Pt thin films was coupled with 0.2LSCO thin films to form TFTCs with a U-pattern. Finally, the fabricated TFTCs were pasted with copper wires at the cold end using silver paste, and then heated at 200 °C for 1 h to make the bonds strong. The output voltages of the TFTCs were measured by a lab-made testing measurement system, similar to our previous work [20]. A muffle furnace (LHT 02/17/P310, Nabertherm, Lilienthal, Germany) was used to provide various temperature differences. The temperature of the hot-junction was collected by a Type-S thermocouple, and the temperature of the cold-end was measured by a Type-K thermocouple at the same time. In order to maintain the reproducibility of the measurement system, the cold-end was chilled and the temperature was kept at 25 °C with circulating water during the experiments, while the hot-junction was fixed in the same place in the furnace. The data of temperatures and output voltages were recorded simultaneously by using a USB Data Acquisition system (LR8431-30, HIOKI, Nagano-ken, Japan) equipped with “Logger Utility” software.

3. Results

To withstand high temperatures for a long time, the 0.2LSCO thin films were deposited for 4 h by using a sputtering system (where the RF power was 150 W, the target diameter was 101.6 mm, the gas pressure was 1.3 Pa, and the O₂/Ar ratio was 0.13/1.17), and then a post-annealing process was carried out from 800 °C to 1300 °C for 1 h. The XRD patterns of different post-annealing temperatures for 0.2LSCO thin films are shown in Figure 1. For the as-deposited 0.2LSCO thin film, only the characteristic peaks of the alumina substrate can be observed, which shows that the film was amorphous. When the post-annealing temperature was 800 °C, the characteristic peaks of 0.2LSCO appeared, and its intensity increased with temperature from 800 °C to 1000 °C, which indicates that a higher temperature was beneficial for the crystallinity of the 0.2LSCO thin film. Conversely, when the post-annealing temperature increased to 1100 °C and 1200 °C, the peaks of impurity phases of Cr₂O₃ marked as spades were observed due to the volatilization of strontium lanthanum chromate above 1000 °C [34]. Moreover, the peaks of Cr₂O₃ disappeared and the peaks of SrCr₂O₇ were observed for the sample post-annealed at 1300 °C, which may be attributed to the secondary combination after the decomposition of the constituent elements for the 0.2LSCO thin film at high temperatures.

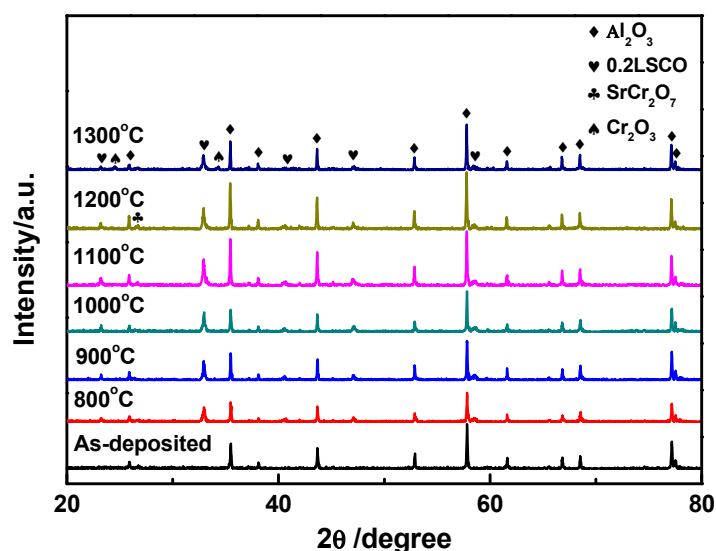


Figure 1. XRD patterns of 0.2LSCO thin films at different post-annealing temperatures.

The surface morphologies of 0.2LSCO thin films post-annealed at different temperatures were measured, and their SEM images are shown in Figure 2a–e. The grain size of the films with different temperatures was obtained by means of the standard root-mean-square method from the SEM images, and the results are shown in Figure 2h. In Figure 2a, for the as-deposited 0.2LSCO thin film, the morphology mainly consisted of grains of the alumina substrate, and the surface of the alumina substrate was uneven, which was due to the amorphous structure of the 0.2LSCO thin film. When the post-annealing temperature reached 800 °C, the surface morphology of the 0.2LSCO thin film was totally different from its as-deposited stage, and a lot of tiny spindle structures could be observed, as shown in Figure 2b, which indicates that the 0.2LSCO thin film was not crystalline. With the increases in post-annealing temperature, the grain size of the 0.2LSCO thin film increased significantly from 0.2 μm at 800 °C to 0.71 μm at 1100 °C, as shown in Figure 2h.

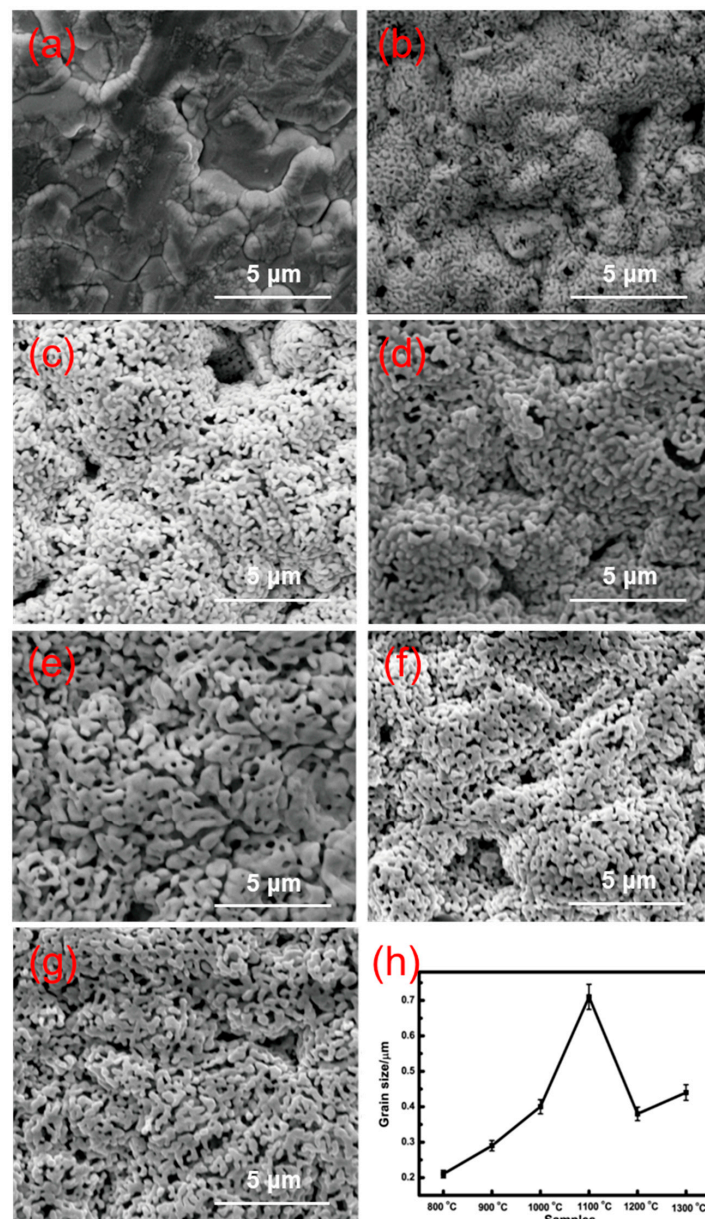


Figure 2. Surface morphologies of 0.2LSCO thin films annealed at different temperatures: (a) deposited; (b) 800 °C; (c) 900 °C; (d) 1000 °C; (e) 1100 °C; (f) 1200 °C; (g) 1300 °C; (h) the change in grain size with different post-annealing temperatures.

The SEM images of cross-sections at different annealing temperatures are shown in Figure 3. The statistical average thicknesses of 0.2LSCO thin films post-annealed at different temperatures were measured from the SEM images, and the changing curve of thicknesses is shown in Figure 3h. For the as-deposited 0.2LSCO thin film, its thickness was about 2.0 μm . The thickness increased slightly with the annealing temperature and reached up to the maximum value of 2.08 μm at 1000 $^{\circ}\text{C}$, which was mainly ascribed to volume expansion induced by the increase in grain size, as shown in Figure 2. However, the thickness decreased significantly when the annealing temperature was higher than 1100 $^{\circ}\text{C}$. The thickness of the 0.2LSCO thin film changed from 1.54 μm at 1100 $^{\circ}\text{C}$ to the minimum value of 1.38 μm at 1300 $^{\circ}\text{C}$, which decreased about 31% compared with that of the as-deposited sample.

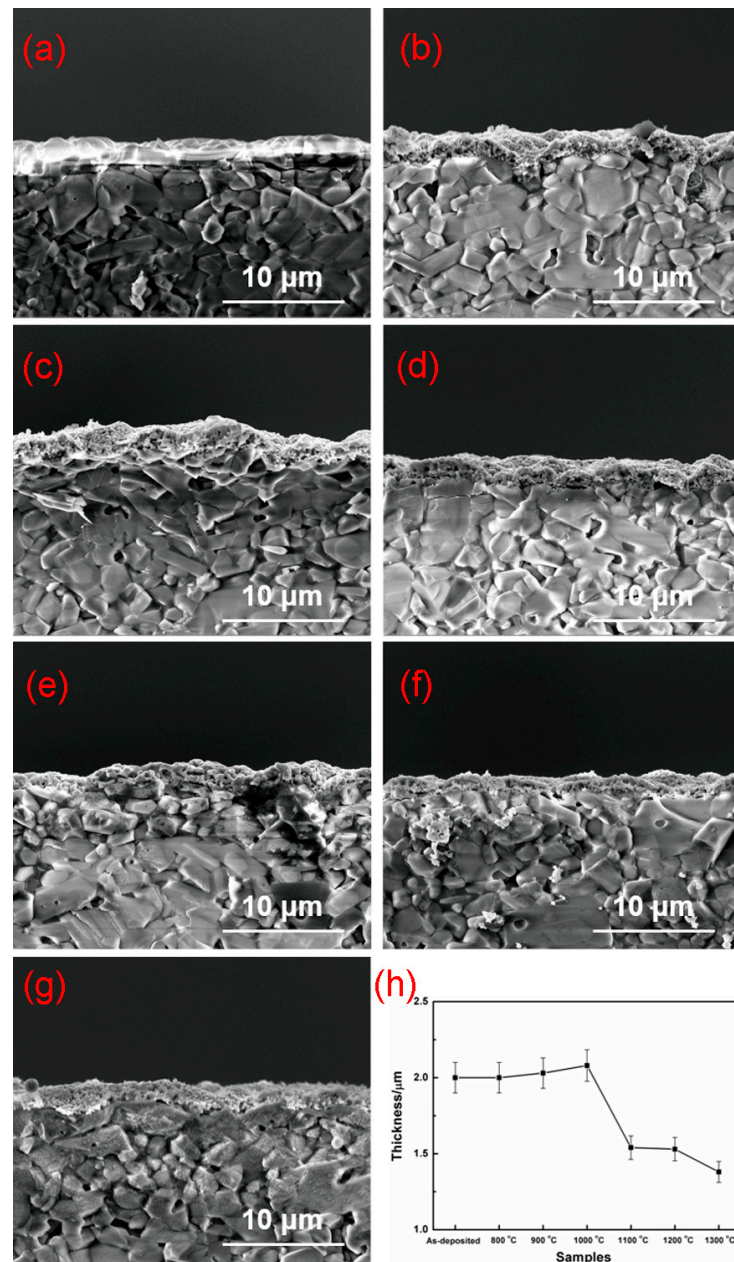


Figure 3. Cross-sections of 0.2LSCO thin films annealed at different temperatures: (a) as-deposited; (b) 800 $^{\circ}\text{C}$; (c) 900 $^{\circ}\text{C}$; (d) 1000 $^{\circ}\text{C}$; (e) 1100 $^{\circ}\text{C}$; (f) 1200 $^{\circ}\text{C}$; (g) 1300 $^{\circ}\text{C}$; (h) the change in thickness.

The constituent elements of the 0.2LSCO thin films post-annealed at different temperatures were measured by EDAX, and the results are shown in Figure 4. Here, the main elemental content of Al, O, La, Sr, and Cr was chosen to analyze the effect of different post-annealing temperatures, and the results are listed in Table 1. The contents of Sr and Cr remained nearly unchanged below 1000 °C, and they then decreased above 1100 °C. For the element La, its content changed slightly even at the post-annealing temperature of 1200 °C, which showed that the evaporation of the 0.2LSCO thin film was mainly in the form of compounds containing elements of Sr and Cr. However, the contents of Sr, La, and Cr decreased significantly for the sample post-annealed at 1300 °C. It is also interesting to note that the content of the Al element had an increasing tendency with the increase in temperature, due to the intensity of aluminum oxide detected with the decreases in the films' thickness.

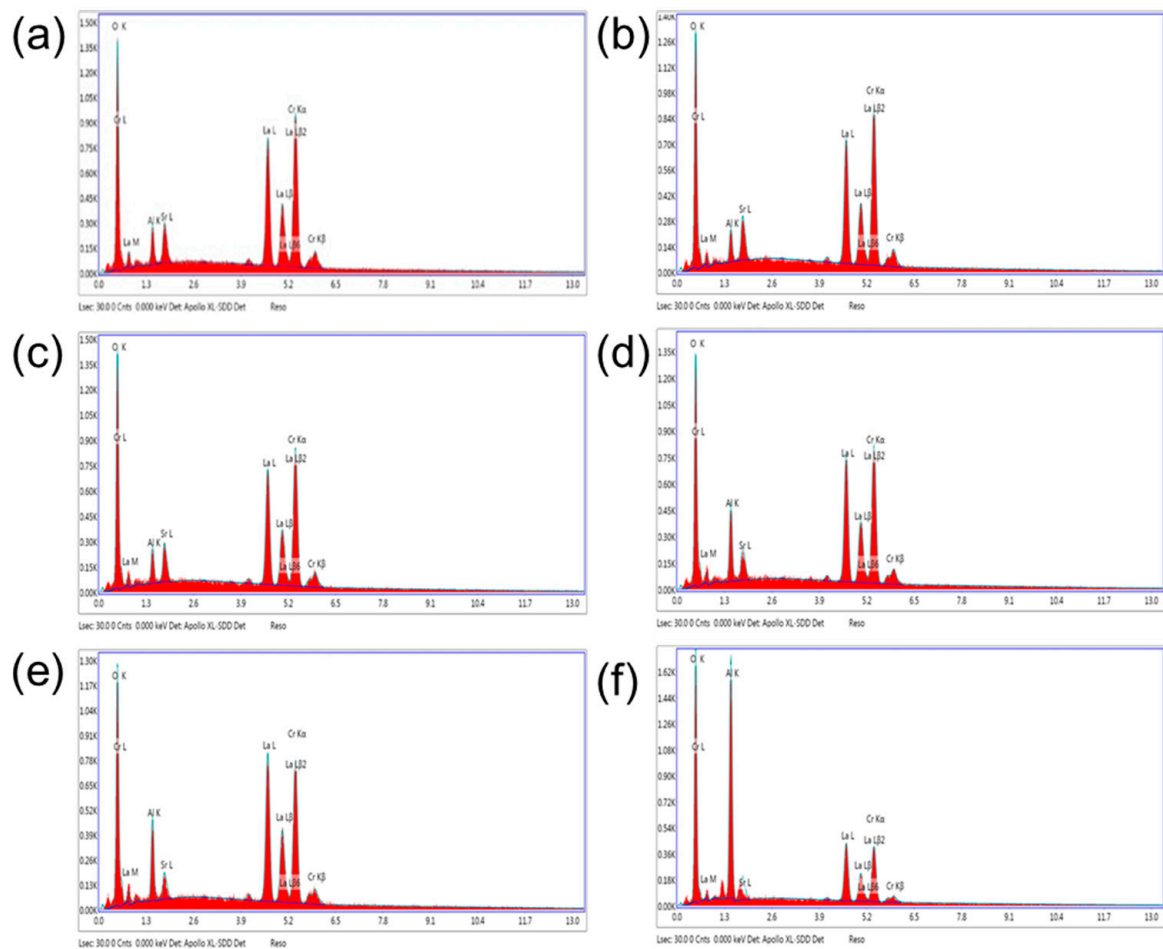


Figure 4. EDAX results of 0.2LSCO thin films annealed at different temperatures for 1 h: (a) 800 °C; (b) 900 °C; (c) 1000 °C; (d) 1100 °C; (e) 1200 °C; (f) 1300 °C.

Table 1. Contents of main elements in 0.2LSCO thin films with different post-annealing temperatures.

Temperature (°C)	Element Atomic Ratio (%)				
	O	Al	Sr	La	Cr
800	55.23	6.12	2.76	15.4	20.48
900	57.46	5.14	2.96	12.96	21.48
1000	59.58	5.94	2.7	12.57	19.22
1100	55.24	11.53	2.22	13.06	17.96
1200	54.56	12.07	1.73	14.46	17.17
1300	61.26	25.12	1.42	5.53	6.67

Figure 5 shows the conductivities of 0.2LSCO thin films annealed at different temperatures using the four-point probe method of the Vanderbilt law. There was a tendency of the conductivity to rise first and then decrease, and the maximum value of 6.25×10^{-2} S/cm was obtained for the 0.2LSCO thin film annealed at 1000 °C. For the rising stage, the crystallinity and grain size of the 0.2LSCO thin film increased with the post-annealing temperature, which resulted in a decrease in the scattering among grain boundaries for carriers. Conversely, for the decreasing stage, the thermal volatilization and formation of the nonconductive secondary phase made the conductivity deteriorative and even insulative at 1300 °C. In other words, an appropriate post-annealing temperature will enhance the conductivity of the 0.2LSCO thin film and reduce the volatilization.

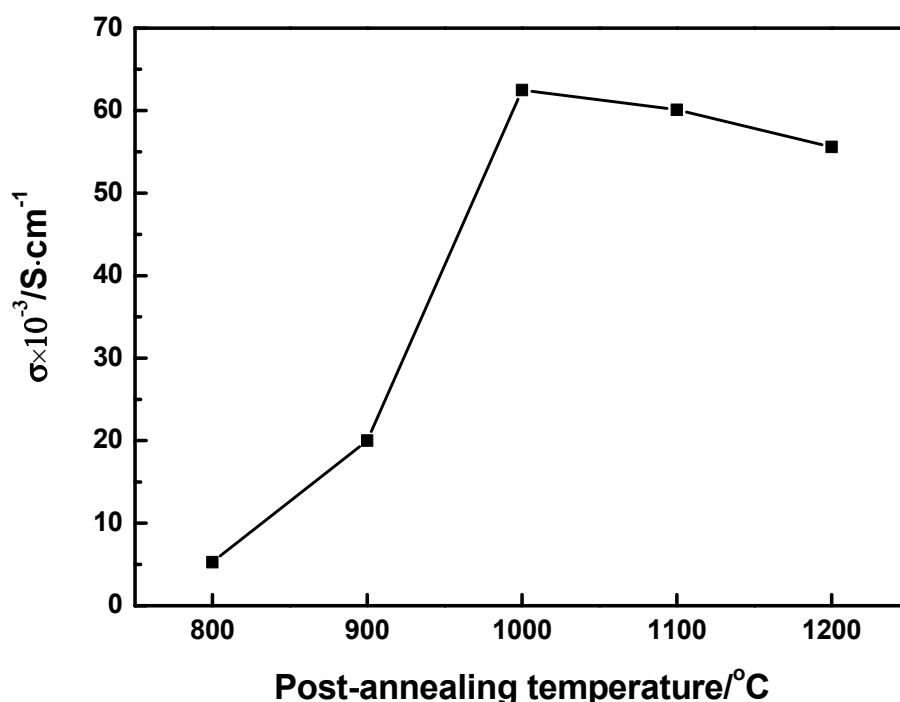


Figure 5. Conductivities of 0.2LSCO thin films at different post-annealing temperatures.

The thermoelectric properties of 0.2LSCO thin films post-annealed at different temperatures were measured by forming U-type TFTCs with Pt thin-film electrodes using a static calibration, and the variation curves of thermal voltages with temperature differences are shown in Figure 6. For the 0.2LSCO thin film annealed at 800 °C, it was difficult to collect the thermal voltages from the voltmeter due to its poor conductivity and lower crystallinity, and its thermal voltage curve has not been marked in this figure. In addition, the thermal voltages have also not been marked for the 0.2LSCO thin film annealed at 1300 °C, because of the interruption of electrical transport of the Pt electrode. For others, their thermal voltages increased first and then decreased with the post-annealing temperature. The results of average Seebeck coefficients of the 0.2LSCO thin films at different post-annealing temperatures are listed in Table 2. The maximum thermal voltage of 167.8 $\mu\text{V}/^\circ\text{C}$ was obtained for the 0.2LSCO thin film annealed at 1100 °C. The reproducibility of the measurements in this lab-made system can be achieved by fixing the place of the hot-junction in the furnace, as well as the temperature at the cold-end, for each test.

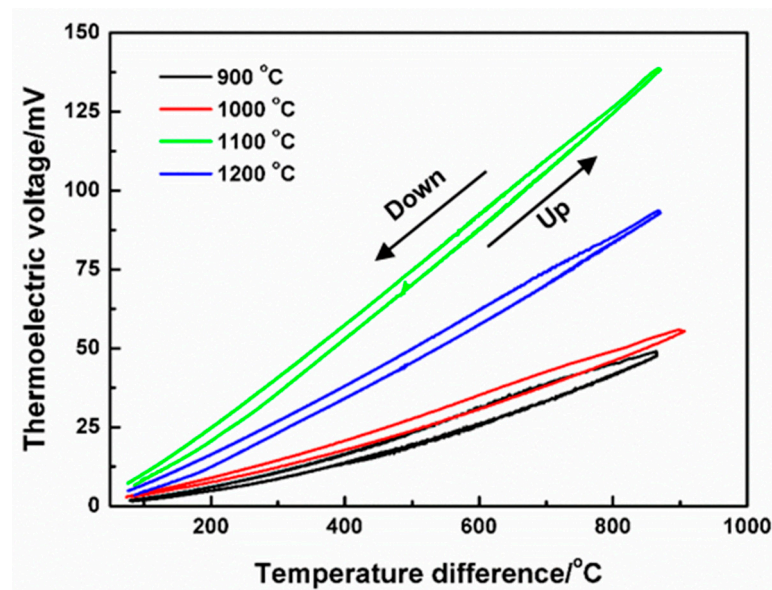


Figure 6. Thermoelectric voltages of 0.2LSCO-Pt TFTCs at different temperature differences.

Table 2. Average Seebeck coefficients of 0.2LSCO thin films at different post-annealing temperatures.

Post-Annealing Temperature (°C)	Seebeck Coefficient ($\mu\text{V}/^\circ\text{C}$)
900	59.0
1000	62.2
1100	167.8
1200	114.1

4. Discussion

From the results of XRD and SEM for 0.2LSCO thin films annealed at different temperatures, the as-deposited 0.2LSCO thin film shows an amorphous structure and needs post-annealing to be suitable as electrodes of TFTCs. When the post-annealing temperature was lower than 800 °C, the amorphous structure was shown in the 0.2LSCO thin film and, accordingly, the crystallization was not good, which agrees with the research results of the literature [35]; a higher temperature over 780 °C should be taken to crystallize chromic acid lanthanum. With the post-annealing temperature increased from 800 °C to 1100 °C, the grain size of the 0.2LSCO thin film increased significantly from 0.2 μm at 800 °C to 0.71 μm at 1100 °C, while the thickness of the films remained stable at about 2.0 μm , indicating the good crystallization of the films. However, when the temperature was higher than 1100 °C, the grain size of the 0.2LSCO thin film decreased with the post-annealing temperature to 1300 °C, while the thickness decreased about 38% at the same time. For this reason, one is due to the emergence of the secondary phases and the intensification of volatilization of Cr_2O_3 and SrCr_2O_7 at higher temperatures; the other is due to the higher specific surface area of the material and the increase in Gibbs free energy, which enhances the reaction between the 0.2LSCO thin film and external thermal environment. Post-annealing treatment will change the morphologies of 0.2LSCO thin films and has an impact on their service stability for high temperatures. Therefore, the post-annealing temperature should be kept below 1100 °C through comprehensive analysis.

In order to obtain optimal parameters for the preparation of thin-film thermocouples, the thermoelectric response with different annealing temperatures was studied accordingly. The maximum thermal voltage of 167.8 $\mu\text{V}/^\circ\text{C}$ was obtained for the 0.2LSCO thin film annealed at 1100 °C. Furthermore, hysteresis phenomena of thermal voltages were observed for all TFTCs between heating and cooling processes because of defect concentration, crystal structure, grain size, and heating rate. On the other hand, it was caused by the formation of a small amount of secondary phase and the decrease in thickness. Conversely, for the

sample annealed at 1200 °C, the thickness of the thin film reduced further due to the enhancement of evaporation, and lower thermal voltages were achieved.

It is well known that the principle of thermocouples is based on the Seebeck effect, which can be defined as Equation (1) [19]:

$$S = \Delta V / \Delta T \quad (1)$$

where S is the Seebeck coefficient, ΔV is the output voltage, and ΔT is the difference temperature between the hot end and cold end. By calculation, the S values of 0.2LSCO-Pt thin-film thermocouples were nearly the same as those of the 0.2LSCO thin films themselves due to the S of Pt being neglected (1.67 V/°C for standard Pt wire [36]). From our previous article [19], the 0.2LSCO thin film annealed at 1000 °C was very stable, and the draft rate of a 0.2LSCO/In₂O₃ TFTC was only 0.58 °C/h, which was almost equal to that of a standard type-K wire thermocouple (0.18 °C/h) with a diameter of 0.5 mm. At the same time, combining with the results of the crystal structure, morphology, and electrical conductivity mentioned above, the post-annealing temperature of 1000 °C was more beneficial for high-temperature sensing. In other words, the post-annealing treatment will affect the microstructure composition, volatilization, and thermoelectric output performance of the 0.2LSCO thin film, and a higher-sensitivity TFTC fabricated by the 0.2LSCO thin film can be achieved to sense high temperatures in air.

5. Conclusions

La_{0.8}Sr_{0.2}CrO₃ thin films were prepared via the RF sputtering method and post-annealed at different temperatures. 0.2LSCO thin films with a pure phase were obtained and the intensity of XRD peaks increased with the temperature from 800 °C to 1000 °C, while impurity phases of Cr₂O₃ and SrCr₂O₇ appeared above 1000 °C. Meanwhile, the grain sizes of 0.2LSCO thin films had a tendency to increase first and then decrease, and the maximum size was 0.71 μm for the thin film post-annealed at 1100 °C due to the apparent melting and agglomerating phenomena. The thicknesses of 0.2LSCO thin films decreased significantly above 1000 °C due to the evaporation of Sr²⁺ and Cr³⁺. The conductivities of 0.2LSCO thin films increased first and then decreased, with a maximum value of 6.25×10^{-2} S/cm obtained for the post-annealing temperature of 1000 °C, while the thermal volatilization and the formation of a nonconductive secondary phase made the conductivity deteriorative at 1300 °C. By coupling with Pt reference electrodes to form TFTCs, the maximum average Seebeck coefficient of 167.8 μV/°C was achieved for the 0.2LSCO thin film annealed at 1100 °C. The results indicated that the properties of the 0.2LSCO thin film can be affected by post-annealing temperature significantly, and an appropriate treatment should be taken to make the 0.2LSCO thin film more stable to fabricate TFTCs for sensing at high temperatures.

Author Contributions: Formal analysis, D.L., P.S., W.R. and B.T.; investigation, D.L., Y.L. and Y.Z.; writing—original draft preparation, D.L.; writing—review and editing, D.L. and P.S. All authors have read and agreed to the published version of the manuscript.

Funding: This research was funded by the National Natural Science Foundation of China (No. 62001428), National Key Research and Development Program of China (No. 2019YFB2004800, No. 2018YFF0212301), Shanxi “1331 Project” Key Subject Construction (1331KSC), Key Research and Development Program of Shaanxi (program No.2021G Y-295), Science Foundation of North University of China (No. XJJ201911), and Scientific and Technological Innovation Programs of Higher Education Institutions in Shanxi (STIP).

Acknowledgments: We also appreciate the support from the International Joint Laboratory for MicroNano Manufacturing and Measurement Technologies.

Conflicts of Interest: The authors declare no conflict of interest.

References

1. Zhang, Z.; Tian, B.; Yu, Q.; Shi, P.; Lin, Q.; Zhao, N.; Jing, W.; Jiang, Z. Range Analysis of Thermal Stress and Optimal Design for Tungsten-Rhenium Thin Film Thermocouples Based on Ceramic Substrates. *Sensors* **2017**, *17*, 857. [[CrossRef](#)] [[PubMed](#)]
2. Zhao, N.; Lin, Q.; Jing, W.; Jiang, Z.; Wu, Z.; Yao, K.; Tian, B.; Zhang, Z.; Shi, P. High temperature high sensitivity Mach-Zehnder interferometer based on waist-enlarged fiber bitapers. *Sens. Actuators A Phys.* **2017**, *267*, 491–495. [[CrossRef](#)]
3. Srinivasan, K.; Sundararajan, T.; Narayanan, S.; Jothi, T.J.S.; Rohit Sarma, C.S.L.V. Acoustic pyrometry in flames. *Measurement* **2013**, *46*, 315–323. [[CrossRef](#)]
4. Tian, B.; Zhang, Z.; Shi, P.; Zheng, C.; Yu, Q.; Jing, W.; Jiang, Z. Tungsten-rhenium thin film thermocouples for SiC-based ceramic matrix composites. *Rev. Sci. Instrum.* **2017**, *88*, 015007. [[CrossRef](#)] [[PubMed](#)]
5. Choi, H.; Li, X. Fabrication and application of micro thin film thermocouples for transient temperature measurement in nanosecond pulsed laser micromachining of nickel. *Sens. Actuators A Phys.* **2007**, *136*, 118–124. [[CrossRef](#)]
6. Kreider, K.G.; Gillen, G. High temperature materials for thin-film thermocouples on silicon wafers. *Thin Solid Films* **2000**, *376*, 32–37. [[CrossRef](#)]
7. Liu, S.; Duan, F.L.; Ji, Z.; Xie, Z.; Hong, Z.; Wang, C.; Xie, X. Accurate and Precise Surface Temperature Measurements Up to 1500 °C Using Thin Film Thermocouple Sensors. In Proceedings of the AIAA Scitech 2021 Forum, Virtual Event, 11–15 & 19–21 January 2021.
8. Tian, B.; Liu, Y.; Zhang, Z.; Liu, Z.; Zhao, L.; Lin, Q.; Shi, P.; Mao, Q.; Lu, D.; Jiang, Z. Effect of Annealing on the Thermoelectricity Properties of the WRe26-In₂O₃ Thin Film Thermocouples. *Micromachines* **2020**, *11*, 664. [[CrossRef](#)]
9. Benedict, R.P.; Hoersch, H. *Manual on the Use of Thermocouples in Temperature Measurement*; ASTM: West Conshohocken, PA, USA, 1993.
10. Burgess, D.; Yust, M.; Kreider, K. Transient thermal response of plasma-sprayed zirconia measured with thin-film thermocouples. *Sens. Actuators A Phys.* **1990**, *24*, 155–161. [[CrossRef](#)]
11. Bhatt, H.D.; Vedula, R.; Desu, S.B.; Fralick, G.C. Thin film TiC/TaC thermocouples. *Thin Solid Films* **1999**, *342*, 214–220. [[CrossRef](#)]
12. Samsonov, G.V.; Kislyi, P.S. *High Temperature Nonmetallic Thermocouples and Sheaths*; Consultants Bureau: Southern California, CA, USA, 1967.
13. Von Moll, A.; Behbahani, A.R.; Fralick, G.C.; Wrbanek, J.D.; Hunter, G.W. A Review of Exhaust Gas Temperature Sensing Techniques for Modern Turbine Engine Controls. In Proceedings of the 50th AIAA/ASME/SAE/ASEE Joint Propulsion Conference, Cleveland, OH, USA, 28–30 July 2014.
14. Chen, X.; Gregory, O.J.; Amani, M. Thin-Film Thermocouples Based on the System In₂O₃-SnO₂. *J. Am. Ceram. Soc.* **2010**, *94*, 854–860. [[CrossRef](#)]
15. Kreider, K.G. Thin-film transparent thermocouples. *Sens. Actuators A Phys.* **1992**, *34*, 95–99. [[CrossRef](#)]
16. Kreider, K.G. High temperature silicide thin-film thermocouples. *Mater. Res. Soc. Symp. Proc.* **1993**, *322*, 285–290. [[CrossRef](#)]
17. Liu, D.; Shi, P.; Ren, W.; Liu, Y.; Liu, M.; Niu, G.; Lin, Q.; Tian, B.; Jiang, Z.; Ye, Z.-G. Facile high-performance film thermocouple made of strontium lanthanum chromate for temperature sensing in air. *J. Am. Ceram. Soc.* **2018**, *101*, 4880–4886. [[CrossRef](#)]
18. Liu, D.; Shi, P.; Ren, W.; Liu, Y.; Liu, M.; Zhang, Y.; Lin, Q.; Tian, B.; Jiang, Z.; Ye, Z.-G. Investigation on thermoelectric properties of screen-printed La_{1-x}Sr_xCrO₃-In₂O₃ thermocouples for high temperature sensing. *J. Eur. Ceram. Soc.* **2018**, *38*, 5030–5035. [[CrossRef](#)]
19. Liu, D.; Shi, P.; Ren, W.; Liu, Y.; Liu, M.; Zhang, Y.; Tian, B.; Lin, Q.; Jiang, Z.; Ye, Z.-G. Fabrication and characterization of La_{0.8}Sr_{0.2}CrO₃/In₂O₃ thin film thermocouple for high temperature sensing. *Sens. Actuators A Phys.* **2018**, *280*, 459–465. [[CrossRef](#)]
20. Liu, Y.; Ren, W.; Shi, P.; Liu, D.; Liu, M.; Jing, W.; Tian, B.; Ye, Z.-G.; Jiang, Z. Preparation and thermal volatility characteristics of In₂O₃/ITO thin film thermocouple by RF magnetron sputtering. *AIP Adv.* **2017**, *7*, 115025. [[CrossRef](#)]
21. Liu, Y.; Ren, W.; Shi, P.; Liu, D.; Zhang, Y.; Liu, M.; Lin, Q.; Tian, B.; Jiang, Z. Microstructure and thermoelectric properties of In₂O₃/ITO thin film thermocouples with Al₂O₃ protecting layer. *J. Mater. Sci. Mater. Electron.* **2018**, *30*, 1786–1793. [[CrossRef](#)]
22. Liu, Y.; Ren, W.; Shi, P.; Liu, D.; Zhang, Y.; Liu, M.; Ye, Z.-G.; Jing, W.; Tian, B.; Jiang, Z. A Highly Thermostable In₂O₃/ITO Thin Film Thermocouple Prepared via Screen Printing for High Temperature Measurements. *Sensors* **2018**, *18*, 958. [[CrossRef](#)]
23. Zhu, W.; Deevi, S. Development of interconnect materials for solid oxide fuel cells. *Mater. Sci. Eng. A* **2003**, *348*, 227–243. [[CrossRef](#)]
24. Karim, D.P.; Aldred, A.T. Localized level hopping transport in La(Sr)CrO₃. *Phys. Rev. B* **1979**, *20*, 2255–2263. [[CrossRef](#)]
25. Brylewski, T.; Dabek, J.; Przybylski, K.; Morgiel, J.; Rekas, M. Screen-printed (La,Sr)CrO₃ coatings on ferritic stainless steel interconnects for solid oxide fuel cells using nanopowders prepared by means of ultrasonic spray pyrolysis. *J. Power Sources* **2012**, *208*, 86–95. [[CrossRef](#)]
26. Pintossi, D.; Iannaccone, G.; Colombo, A.; Bella, F.; Välimäki, M.; Väisänen, K.L.; Hast, J.; Levi, M.; Gerbaldi, C.; Dragonetti, C.; et al. Luminescent Downshifting by Photo-Induced Sol-Gel Hybrid Coatings: Accessing Multifunctionality on Flexible Organic Photovoltaics via Ambient Temperature Material Processing. *Adv. Electron. Mater.* **2016**, *2*, 1600288. [[CrossRef](#)]
27. Seo, S.; Ryu, J.; Kim, S.; Jeong, J.; Jin, S. Enhancement of Photodetective Properties on Multilayered MoS₂ Thin Film Transistors via Self-Assembled Poly-L-Lysine Treatment and Their Potential Application in Optical Sensors. *Nanomaterials* **2021**, *11*, 1586. [[CrossRef](#)]
28. Bella, F.; De Luca, S.; Fagiolarì, L.; Versaci, D.; Amici, J.; Francia, C.; Bodoardo, S. An Overview on Anodes for Magnesium Batteries: Challenges towards a Promising Storage Solution for Renewables. *Nanomaterials* **2021**, *11*, 810. [[CrossRef](#)] [[PubMed](#)]

29. Pugliese, D.; Lamberti, A.; Bella, F.; Sacco, A.; Bianco, S.; Tresso, E. TiO₂ nanotubes as flexible photoanode for back-illuminated dye-sensitized solar cells with hemi-squaraine organic dye and iodine-free transparent electrolyte. *Org. Electron.* **2014**, *15*, 3715–3722. [[CrossRef](#)]
30. Sacco, A.; Bella, F.; Pierre, S.D.; Castellino, M.; Bianco, S.; Bongiovanni, R.; Pirri, C.F. Electrodes/Electrolyte Interfaces in the Presence of a Surface-Modified Photopolymer Electrolyte: Application in Dye-Sensitized Solar Cells. *Chem. Phys. Chem.* **2015**, *16*, 960–969. [[CrossRef](#)]
31. Campbell, I.A.; Turnbull, G.A. A kinetic model of thin-film fluorescent sensors for strategies to enhance chemical selectivity. *Phys. Chem. Chem. Phys.* **2021**, *23*, 10791–10798. [[CrossRef](#)] [[PubMed](#)]
32. Liang, Q.; Liu, H.; Wang, C.; Li, B. Phenotypic Characterization Analysis of Human Hepatocarcinoma by Urine Metabolomics Approach. *Sci. Rep.* **2016**, *6*, 19763. [[CrossRef](#)]
33. Liu, D.; Shi, P.; Ren, W.; Liu, Y.; Liu, M.; Zhang, Y.; Tian, B.; Lin, Q.; Jiang, Z.; Ye, Z.-G. Enhanced La_{0.8}Sr_{0.2}CrO₃/Pt thin film thermocouple with Al₂O₃ coating layer for high temperature sensing. *Ceram. Int.* **2018**, *44*, S233–S237. [[CrossRef](#)]
34. Mori, M.; Yamamoto, T.; Ichikawa, T.; Takeda, Y. Dense sintered conditions and sintering mechanisms for alkaline earth metal (Mg, Ca and Sr)-doped LaCrO₃ perovskites under reducing atmosphere. *Solid State Ion.* **2002**, *148*, 93–101. [[CrossRef](#)]
35. Johnson, C.; Gemmen, R.; Orlovskaya, N. Nano-structured self-assembled LaCrO₃ thin film deposited by RF-magnetron sputtering on a stainless steel interconnect material. *Compos. Part B Eng.* **2004**, *35*, 167–172. [[CrossRef](#)]
36. ASTM E230/E230M-12. *Standard Specification and Temperature Electromotive Force (emf) Tables for Standardized Thermocouples*; ASTM International: West Conshohocken, PA, USA, 2012.